Self-organization of shallow basins in tidal flats and salt marshes

A. Defina,[1] L. Carniello,[1] S. Fagherazzi,[2] and L. D'Alpaos[1]

[1] Shallow tidal basins such as the Venice Lagoon, Italy, are often characterized by extensive tidal flats and salt marshes that lie within specific ranges of elevation. Tidal flats lie just below the mean sea level, approximately between -0.6 and -2.0 meters above the mean sea level (m a.m.s.l.), whereas salt marshes lie at an average elevation higher than mean sea level (i.e., between $+0.1$ and $+0.5$ m a.m.s.l.). Only a small fraction of the tidal basin area has elevations between -0.6 and $+0.1$ m a.m.s.l. This occurrence suggests that the morphodynamic processes responsible for sediment deposition and erosion produce either tidal flats or salt marshes but no landforms located in the above intermediate range of elevations. A conceptual model describing this evolutionary trend has recently been proposed. The model assumes that the bimodal distribution of bottom elevations stems from the characteristics of wave induced sediment resuspension and demonstrates that areas at intermediate elevations are inherently unstable and tend to become either tidal flats or salt marshes. In this work, the conceptual model is validated through comparison with numerical results obtained with a two-dimensional wind wave-tidal model applied to the Lagoon of Venice, Italy. Both the present and the 1901 bathymetries of the Venice Lagoon are used in the simulations and the obtained numerical results confirm the validity of the conceptual model. A new framework that explains the long-term evolution of shallow tidal basins based on the results presented herein is finally proposed and discussed.

1. Introduction

[2] Shallow tidal basins are often characterized by extensive tidal flats and marshes dissected by an intricate network of channels [*Rinaldo et al.*, 1999a, 1999b; *Fagherazzi et al.*, 1999; *Defina*, 2000; *Marani et al.*, 2003]. Both tidal flats and salt marshes are prevalently flat landforms located in the intertidal zone. Tidal flats lie below mean sea level, and only the lowest tides expose their surface. Salt marshes have an elevation higher than the mean sea level, are flooded during high tides, and sustain a dense vegetation canopy of halophyte plants that withstand the relative infrequent flooding periods.

[3] A typical intertidal landscape can be found in the Venice Lagoon, Italy, where tidal flats and salt marshes are separated by a well-defined scarp. The distribution of elevations in the Venice Lagoon shows that tidal flats have differences in elevation of few tens of centimeters, with an average elevation between -0.6 and -2.0 meters above the mean sea level (m a.m.s.l.), whereas salt marshes lie at an average elevation higher than $+0.1$ m a.m.s.l., with some

variability dictated by local sedimentological and ecological conditions. Few areas are located at intermediate elevations (i.e., between -0.6 m and $+0.1$ m a.m.s.l.), suggesting that the processes responsible for sediment deposition and erosion produce either tidal flats or salt marshes but few landforms located in the above critical range of elevations.

[4] Salt marshes directly form from tidal flats in locations where sedimentation is enhanced by lower tidal velocities, by higher sediment concentrations, or by the sheltering effects of spits and barrier islands [*Dijkema*, 1987; *Allen*, 2000]. Typical conceptual and numerical models of marsh formation envision a gradual transition through sediment build-up and plant colonization from sandflats and mudflats [*Beeftink*, 1966; *French and Stoddart*, 1992; *Fagherazzi and Furbish*, 2001; *D'Alpaos et al.*, 2006]. Conversely, in areas with consistent sediment resuspension, tidal flats are dominant because sediment deposition is balanced by erosion and the bottom elevation is constantly maintained below mean sea level [*Allen and Duffy*, 1998].

[5] The role of sediment resuspension by wind waves is often decisive in shallow tidal basins, whereas tidal fluxes alone are unable to produce the bottom shear stresses necessary to mobilize tidal flat sediments [*Carniello et al.*, 2005]. Tidal currents drive morphological evolution only in the channels and in deep areas where the corresponding shear stresses are high enough to resuspend sediments. In shallow areas, tidal currents are instead important in enhancing the

---

[1]Dipartimento di Ingegneria Idraulica, Marittima, Ambientale e Geotecnica (IMAGE), Universitá di Padova, Padova, Italy.
[2]Department of Geological Sciences and School of Computational Science, Florida State University, Tallahassee, Florida, USA.

bottom shear stress due to wind waves because the nonlinear interaction between the wave and current boundary layers increase the shear stress beyond the sum of the two singular contributions [*Soulsby*, 1995, 1997].

[6] A conceptual model explaining the transition between tidal flats and salt marshes has recently been proposed by *Fagherazzi et al.* [2006]. The model shows that areas with elevations in the critical range (i.e., between −0.6 m and +0.1 m a.m.s.l. for the Lagoon of Venice) are inherently unstable and tend to become either tidal flats or salt marshes. In the present paper, the above conceptual model is validated using the results of a complete coupled wind wave-tidal model. Both models are shortly described before discussion.

2. Mathematical Models

2.1. Wind Wave-Tidal Model

[7] Before introducing the conceptual model suggested by *Fagherazzi et al.* [2006] to explain the ubiquitous scarcity of areas located at intermediate elevations between tidal flats and salt marshes, we describe the coupled wind wave-tidal model used to validate the conceptual model [*Carniello et al.*, 2005].

[8] The coupled wind wave-tidal model is composed of a hydrodynamic module and a wind wave module. The hydrodynamic module solves the two-dimensional shallow-water equations modified to deal with flooding and drying processes in irregular domains [*Defina et al.*, 1994; *D'Alpaos and Defina*, 1995]. The presence of bottom irregularities, which strongly affect the hydrodynamics in very shallow flows, is considered in the model from a statistical point of view [*Defina*, 2000]. The two-dimensional equations solved by the hydrodynamic model are as follows:

$$\frac{\partial q_x}{\partial t} + \frac{\partial}{\partial x}\left(\frac{q_x^2}{Y}\right) + \frac{\partial}{\partial y}\left(\frac{q_x q_y}{Y}\right) - \left(\frac{\partial R_{xx}}{\partial x} + \frac{\partial R_{xy}}{\partial y}\right) \\ + \frac{\tau_{bx}}{\rho} - \frac{\tau_{wx}}{\rho} + g\,Y\,\frac{\partial h}{\partial x} = 0 \quad (1)$$

$$\frac{\partial q_y}{\partial t} + \frac{\partial}{\partial x}\left(\frac{q_x q_y}{Y}\right) + \frac{\partial}{\partial y}\left(\frac{q_y^2}{Y}\right) - \left(\frac{\partial R_{xy}}{\partial x} + \frac{\partial R_{yy}}{\partial y}\right) \\ + \frac{\tau_{by}}{\rho} - \frac{\tau_{wy}}{\rho} + g\,Y\,\frac{\partial h}{\partial y} = 0 \quad (2)$$

$$\eta\,\frac{\partial h}{\partial t} + \frac{\partial q_x}{\partial x} + \frac{\partial q_y}{\partial y} = 0 \quad (3)$$

where t denotes time; q_x, q_y are the flow rates per unit width in the x, y (planform) directions, respectively; R_{ij} is the Reynolds stresses (i, j denoting either the x or y co-ordinates); $\tau_{b,curr}$ is the stress at the bottom produced by the tidal current, equal to (τ_{bx}, τ_{by}); τ_w is the wind shear stress at the free surface, equal to (τ_{wx}, τ_{wy}); ρ is fluid density; h is free surface elevation; and g is gravity. Y is the effective water depth, defined as the volume of water per unit area actually ponding the bottom and η is the local fraction of wetted domain and accounts for the actual area that is wetted or dried during the tidal cycle [*Defina*, 2000].

[9] For the case of a turbulent flow over a rough wall, the bed shear stress can be written as:

$$\frac{\tau_{b,curr}}{\rho\,Y} = g\left(\frac{|\boldsymbol{q}|}{k_S^2 D^{10/3}}\right)\boldsymbol{q} \quad (4)$$

where $\boldsymbol{q} = (q_x, q_y)$, $|\boldsymbol{q}| = \sqrt{q_x^2 + q_y^2}$, k_S is the Strickler bed roughness coefficient, and D is an equivalent water depth [*Defina*, 2000].

[10] A semi-implicit staggered finite element method based on Galerkin's approach is used to implement the model [*D'Alpaos and Defina*, 1995; *Defina*, 2003]. This numerical scheme is very suitable when dealing with morphologically complex basins such as the Venice Lagoon.

[11] The hydrodynamic model has been tested and validated simulating the propagation of several real tides and comparing the computed water levels and velocities with field data [*D'Alpaos and Defina*, 1993, 1995]. The model performs satisfactorily also when wind action during stormy conditions is considered [*Carniello et al.*, 2005].

[12] At each time step, the hydrodynamic model yields nodal water levels which are used by the wind wave model to assess wave group celerity and bottom influence on wave propagation.

[13] The wind wave module is based on the conservation of the wave action [*Hasselmann et al.*, 1973], which is defined as the ratio of wave energy density E to the wave frequency σ.

[14] For the case of shallow closed basins, the general spectral formulation of the wave action conservation equation can be simplified. In accordance with *Carniello et al.* [2005], we assume a monochromatic wave and neglect nonlinear wave-wave and wave-current interactions such that σ is constant both in space and in time. We further assume that the direction of wave propagation instantaneously adjusts to the wind direction. The wave action conservation equation can thus be written as:

$$\frac{\partial E}{\partial t} + \frac{\partial}{\partial x}c_{gx}E + \frac{\partial}{\partial y}c_{gy}E = S \quad (5)$$

[15] The first term of (5) represents the local rate of change of wave energy density in time, the second and third terms represent the energy convection (c_{gx} and c_{gy} are the x and y components of the wave group celerity). The source term S on the right-hand side of (5) describes all the external contributions to wave energy and can be either positive, for example, wind energy input, or negative, for example, energy dissipation by bottom friction, whitecapping, and depth-induced breaking. Table 1 summarizes the source terms formulations implemented in the model.

[16] Equation (5) is solved with an upwind finite volume scheme, which uses the same computational grid as the hydrodynamic model. The wind wave model computes the wave energy in each computational element at each time step. The significant wave height H is then computed using the linear theory

$$H = \sqrt{8E/(\rho g)} \quad (6)$$

Table 1. Formulation for Wave Generation and Dissipation [After *Booij et al.*, 1999]

Wind Generation	$S_w = \alpha + \beta \times E$	$\alpha(k) = \frac{80\rho_a^2\sigma}{\rho g k^2}c_d^2 U^4$	k: wave number; $\sigma = 2\pi/T$ (T is wave period); ρ_a: air density; ρ: water density; c_d: drag coefficient, $\cong 0.0012$;
		$\beta(k) = 5\frac{\rho_a}{\rho}\frac{\sigma}{2\pi}(\frac{U_w\cos\delta}{c} - 0.90)$	U: the wind speed (m/s); δ: angle between wind and wave vector; $c = \sigma/k$ wave celerity.
Bottom Friction		$S_{bf} = -4c_{bf}\frac{\pi H}{T}\frac{k}{\sinh(kY)\sinh(2kY)}E$	H: significant wave height Y: water depth; $c_{bf} = 0.015$.
Whitecapping		$S_{wc} = -c_{wc}\sigma(\frac{\gamma}{\gamma_{PM}})^m E$	γ: integral wave-steepness parameter, equal to $E\sigma^4/g^2$); γ_{PM}: theoretical value of γ for a Pearson-Moskowitz spectrum, equal to 4.57×10^{-3}; $c_{wc} = 3.33 \times 10^{-5}$.
Breaking		$S_{brk} = \frac{2}{T}Q_b(\frac{H_{max}}{H})^2 E$	H_{max}: maximum wave height, equal to $0.78Y$; Q_b: breaking probability.

[17] Both tidal currents and wind waves contribute to the production of bottom shear stresses. Equation (4) is used to evaluate the tidal current contribution ($\tau_{b,curr}$). Bottom shear stress due to waves ($\tau_{b,wave}$) is computed as

$$\tau_{b,wave} = \frac{1}{2}f_w\rho u_m^2 \quad \text{with} \quad u_m = \frac{\pi H}{T\,\sinh(kY)} \quad \text{and}$$
$$f_w = 1.39\left[\frac{u_m T}{2\pi(D_{50}/12)}\right]^{-0.52} \tag{7}$$

[18] Here u_m is the maximum horizontal orbital velocity at the bottom, Y is the effective water depth, f_w is the wave friction factor, T is the wave period, k is the wave number, and D_{50} is the median grain diameter.

[19] Actual bed shear stress under the combined action of waves and currents is enhanced beyond the sum of the two contributions. This occurs because of the interaction between the wave and current boundary layers. In the coupled model, the empirical formulation suggested by *Soulsby* [1995, 1997] is adopted. Accordingly, the mean bed shear stress τ_{bm} is as follows:

$$\tau_{bm} = \tau_{b,curr}\left[1 + 1.2\left(\frac{\tau_{b,wave}}{\tau_{b,curr} + \tau_{b,wave}}\right)^{3.2}\right] \tag{8}$$

[20] The maximum shear stress (τ_b), due to the combined action of waves and currents, is given as a vector addition of τ_m and shear stress induced by waves [*Soulsby*, 1997]:

$$\tau_b = \left[\left(\tau_{bm} + \tau_{b,wave}\cos\phi\right)^2 + \left(\tau_{b,wave}\sin\phi\right)^2\right]^{1/2} \tag{9}$$

where ϕ is the angle between the current and the wave directions. Since maximum shear stress τ_b, rather than average stress τ_{bm}, is responsible for bottom sediments mobilization, the results presented and discussed herein utilize the maximum total bottom shear stress.

2.2. Conceptual Model

[21] Based on the above wave formulation, a conceptual model to describe the critical bifurcation of tidal basins

landforms in tidal flats and salt marshes has recently been proposed by *Fagherazzi et al.* [2006]. The model is here shortly described.

[22] In shallow basins, waves quickly adapt to external forcing (that is, the local rate of change of wave energy becomes negligible in a short period of time) and the fetch required to attain fully developed condition is short (a fetch length of 2000 ∼ 3000 m is sufficient for water depths around 1 m). The latter implies that energy transfer, described by the convective terms in equation (5) poorly contributes to energy balance in open areas. Therefore as a first approximation, the conservation equation (5) can be reduced to the local equilibrium between the energy generated by the wind action (S_w) and the energy dissipated by bottom friction (S_{bf}), whitecapping (S_{wc}) and breaking (S_{brk}) (see Table 1 for source terms formulation):

$$S_w = S_{bf} + S_{wc} + S_{brk} \tag{10}$$

[23] Shear stresses produced by wind waves are limited in shallow waters due to dissipative processes. However, they are also limited in deep water where the bottom is too deep to be affected by wave oscillations. Therefore plotting the equilibrium shear stress at the bottom as a function of water depth we obtain a curve peaking at some intermediate water depth (Figure 1). It is worth noting that the depth at which the shear stress is maximized is weakly affected by wind speed [*Fagherazzi et al.*, 2006].

[24] This maximum in shear stress bears important consequences for the morphological transition from tidal flats to salt marshes and for the overall redistribution of sediments in shallow coastal basins.

[25] The model assumes that the rate of sediment erosion E_S is proportional to the difference between bottom shear stress (τ_b) and the critical shear stress for sediment erosion (τ_{cr}) [*Fagherazzi and Furbish*, 2001; *Sanford and Maa*, 2001]

$$E_S = E_{S0}(\tau_b/\tau_{cr} - 1)^\alpha \tag{11}$$

where E_{S0} is a suitable specific erosion rate and α ranges between 1 for cohesive sediments and 1.5 for loose
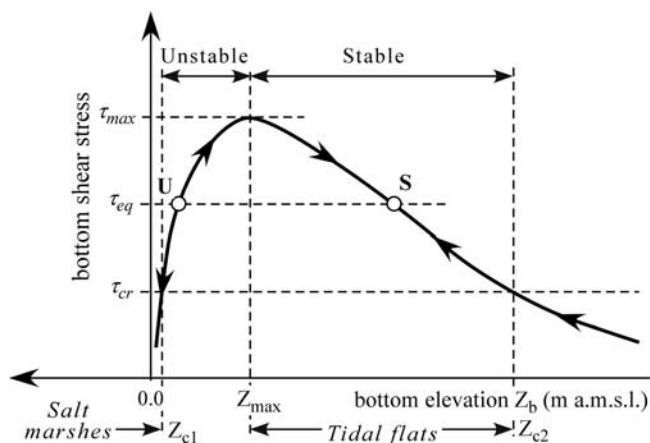
Figure 1. Bed shear stress distribution as a function of bottom elevation.

sediments [*Van Rijn*, 1984; *Mehta et al.*, 1989; *Sanford and Maa*, 2001].

[26] The model further assumes some prescribed average annual sedimentation rate D_S, which is site-dependent, but yet constant during bottom evolution.

[27] Based on the relationship between shear stress and bottom elevation (Figure 1), the conceptual model for the morphological development of salt marshes from tidal flats demonstrates that starting from any initial elevation, the final, equilibrium configuration will be either a salt marsh or a tidal flat deeper than Z_{max} (Figure 1).

[28] When $Z_b < Z_{c2}$, bed shear stress is smaller than the critical shear stress. In this range of depths, we have $E_S = 0$ and $D_S > 0$, thus no equilibrium between deposition and erosion is possible. Therefore tidal flats deeper than Z_{c2} evolve toward smaller depths.

[29] For the same reason, equilibrium is not possible for $Z_b > Z_{c1}$. In this case, deposition will lead to a salt marsh.

[30] Let E_{Smax} be the rate of erosion corresponding to $\tau_b = \tau_{max}$. If deposition is greater than the maximum erosion, i.e., $D_S > E_{Smax}$, then again no equilibrium is possible and vertical accretion of tidal flat will eventually give form to an emergent salt marsh. Once the tidal flat shoals, the accretion dynamics is marginally affected by waves. The main factors determining the final salt marsh elevation are sediment supply, organic production driven by vegetation encroachment [*Silvestri et al.*, 2005], and sediment compaction.

[31] The most interesting range is $\tau_{cr} < \tau_b < \tau_{max}$ and $D_S < E_{Smax}$. In this case, a bed shear stress exists such that $E_S = D_S$ and dynamic equilibrium is possible. We refer to this bed shear stress value as 'equilibrium bed shear stress', τ_{eq} (see Figure 1). The equilibrium bed shear stress marks two points (points U and S) on the curve of Figure 1. When $\tau_b < \tau_{eq}$, deposition exceeds erosion and the bottom evolves toward higher elevations. On the contrary, when $\tau_b > \tau_{eq}$, erosion exceeds deposition and the bottom evolves toward lower elevations. This behavior is marked with the arrows flowing along the curve in Figure 1. It is clear that any point S on the right branch of the curve with $Z_{max} < Z_b < Z_{c2}$ is a stable point: any small departure from point S meets conditions that drive back the bottom elevation toward equilibrium. Any point U on the left branch of the curve

with $Z_{c1} < Z_b < Z_{max}$ is an unstable point: any small departure from point U meets conditions that drive the bottom elevation further away from equilibrium.

[32] Therefore a stable morphodynamic equilibrium is possible in the ranges $Z_b < Z_{c1}$ pertaining to salt marshes and $Z_{max} < Z_b < Z_{c2}$ pertaining to tidal flats.

[33] The presence of an unstable branch in the curve of Figure 1 (i.e., $Z_{c1} < Z_b < Z_{max}$) is a very reasonable explanation for the reduced frequency of areas at these intermediate elevations.

[34] *Fagherazzi et al.* [2006] also discuss the case of depth-dependent deposition rate and show that the main conclusions are not altered.

[35] It is worth stressing that the model assumes that (1) the wind waves are the main source of bottom shear stress (i.e., the model does not apply to tidal channels where bottom shear stress is mainly due to tidal current) and (2) the wavefield is locally fully developed (fetch-limited conditions are discussed in the study of *Fagherazzi et al.* [2006]).

3. Application to the Lagoon of Venice

[36] The results of two numerical simulations performed with the wind wave-tidal model are used to test the above conceptual model. The first simulation uses a refined mesh that reproduces the present bathymetry of the Lagoon of Venice, the second simulation uses the bathymetry of 1901 which is far different from the modern one.

3.1. 2000 Bathymetry

[37] In the first simulation a real meteorological event (16–17 February 2003) characterized by Bora wind blowing from North-East at an average speed of approximately 10 m/s is simulated. The recorded tidal levels shown in Figure 2 are imposed at the three inlets. These tidal and meteorological conditions are representative of a typical, morphologically significant, stormy condition for the Venice Lagoon. Details about the model results are reported in the study of *Carniello et al.* [2005]. The main hydrodynamic results are summarized here in Figure 2.

[38] In the discussion we consider the hydrodynamics computed at $t = 9:00$ P.M. of 16 February 2003 when the water level in the sea is approximately 0.2 m a.m.s.l., but the water levels in the lagoon are around 0.0 m a.m.s.l. due to phase lag.

[39] The analysis is restricted to the central-southern part of the Venice Lagoon (South of the city of Venice) where the condition of fully developed wavefield (required by the conceptual model) is established over most of the domain (Figure 2).

[40] The computed bottom shear stresses are plotted versus bottom elevations in Figure 3.

[41] According to the conceptual model, most of the points should fall along the theoretical curve of Figure 1. Although the points in Figure 3 display a considerable scatter, most of them are indeed clustered along a curve similar to the theoretical one.

[42] To better analyze the model results, the points plotted in Figure 3 are grouped into six regions as shown in Figure 4.
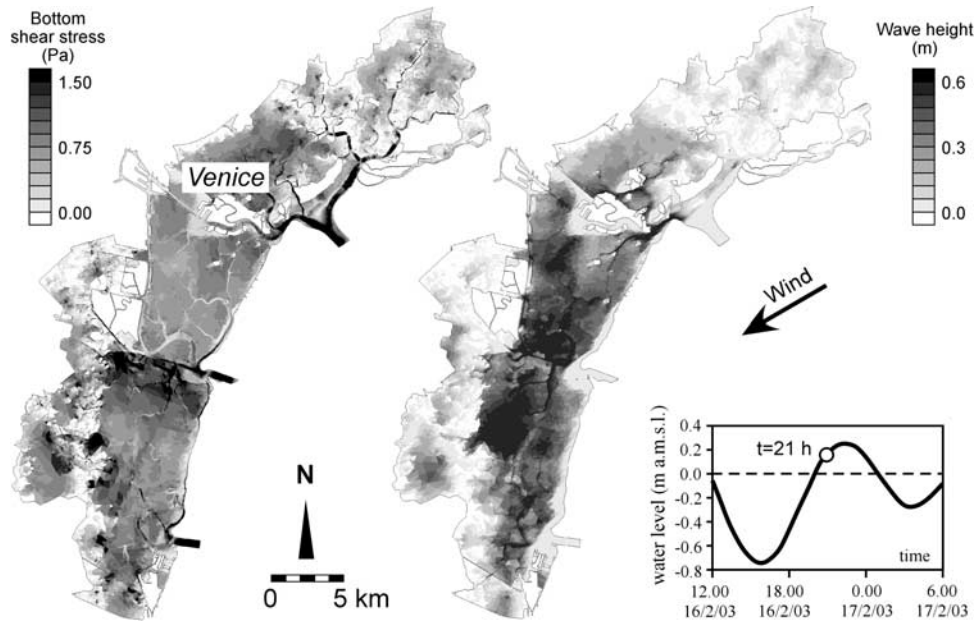
Figure 2. Computed (left) bottom shear stress and (right) wave height distributions on t = 9:00 P.M. of 16 February 2003, during Bora wind.

[43] Curves A and B in Figure 4 define a strip that approximately follows the theoretical curve of Figure 1. Regions *a* to *d*, within the above strip, are bounded by the critical shear stress and the bottom elevation corresponding to the maximum shear stress, Z_{max}.

[44] We also locate the points plotted in Figure 4 on the map of the Venice Lagoon in order to discuss any correlation between the position on the plot and the geographic location.

[45] Points belonging to region 1 have a bottom shear stress considerably lower than that predicted by the conceptual model. This would be consistent with the theory if the limiting effects of fetch length were considered [*Fagherazzi et al.*, 2006]. Therefore points with shear stress and depth falling in region 1 are likely to be located leeward of spits, islands, and emergent salt marshes where fetch length is considerably shorter than the one required to attain fully developed sea.

[46] Figure 5a shows the position of all the points belonging to region 1. As expected, they lie along the boundaries of the lagoon where the wavefield cannot fully develop, and in sheltered areas behind islands and salt marshes where the fetch is limited (cf., Figure 2). Therefore all these points must be removed from the analysis of the conceptual model.

[47] Region 2 comprises points with a bottom shear stress greater than the one predicted by the conceptual model. However, most of these points belong to tidal channels (Figure 5b) where tidal flow concentrates and bed shear stress is mainly due to tidal currents rather than to wind waves. All these point are thus beyond the main assumption of the conceptual model and must be removed from the analysis.

[48] The above results demonstrate that only points falling in the strip between curves A and B must be considered in the discussion of the conceptual model.
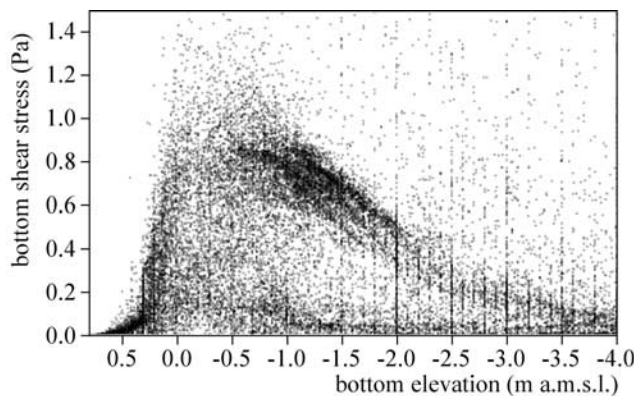
Figure 3. Computed bed shear stress distribution as a function of bottom elevation.
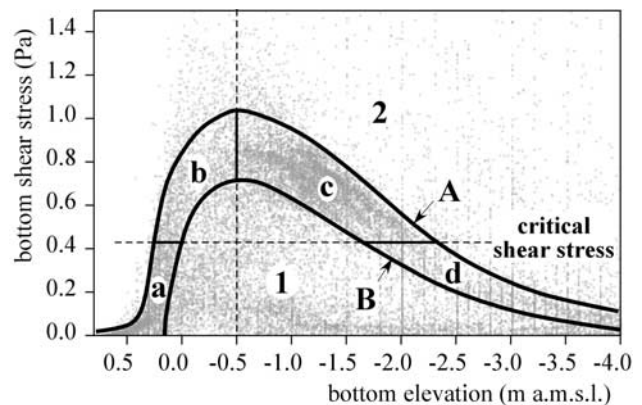
Figure 4. Bed shear stress versus bottom elevation: computed points of Figure 3 are grouped into six regions.
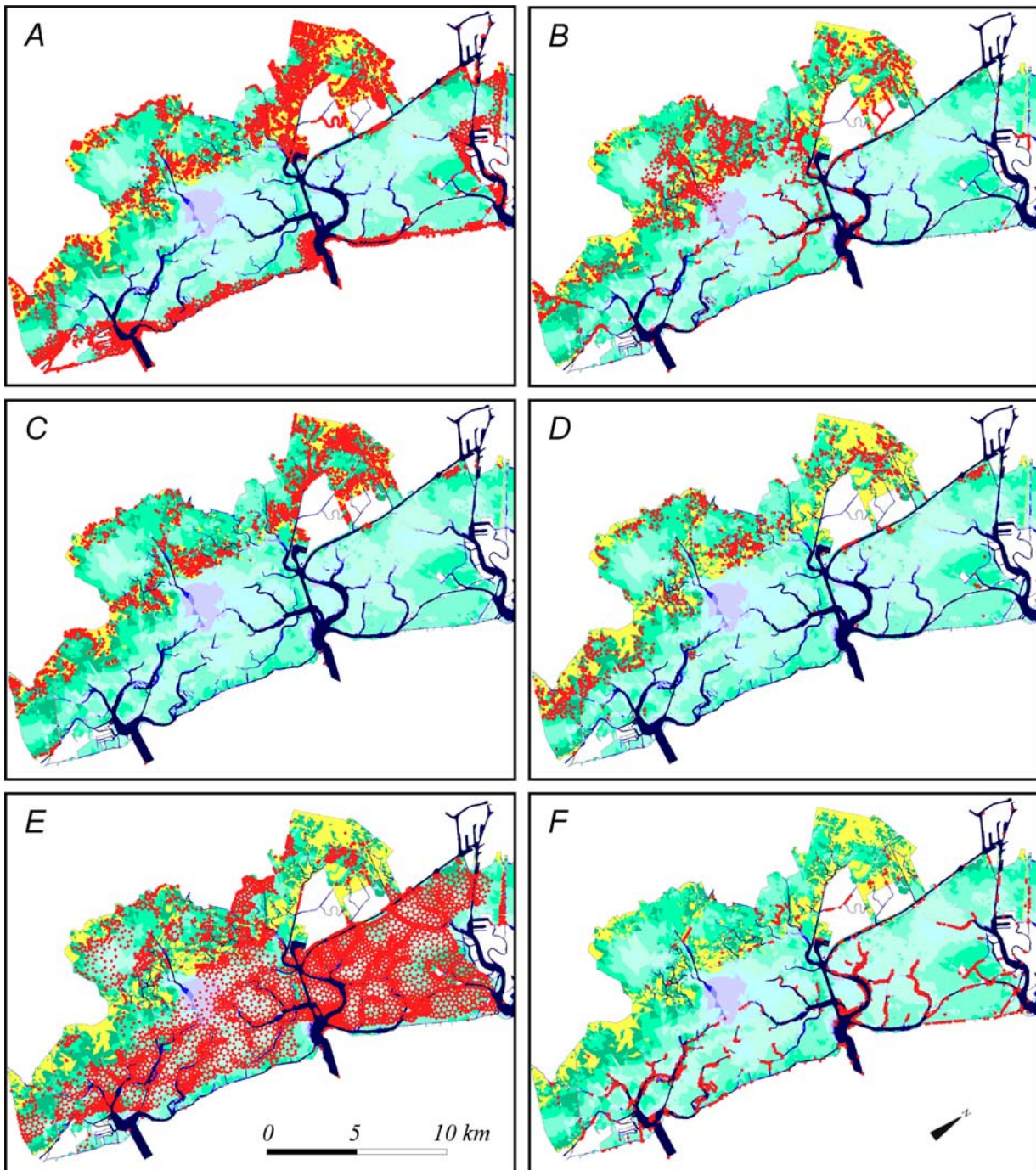
Figure 5. Spatial distribution of basin area following the subdivision indicated in Figure 4: (a) region 1; (b) region 2; (c) region *a*; (d) region *b*; (e) region *c*; (f) region *d* (each point marks the center of a computational element).

[49] Points in region *a* are characterized by a bottom elevation higher than mean sea level. These points are uniformly distributed on salt marshes as shown in Figure 5c.

[50] Points in region *b* belong to the unstable branch of the theoretical curve. According to the conceptual model, few points should fall in this unstable region and they should mark areas in transition from tidal flats to salt marshes or vice versa. As expected, points in region *b* cover an area which is only 9.2% of the total area covered by points in the strip. Moreover, as shown in Figure 5d,

most of these points are located on tidal flats close to salt marsh edges. Here the present lagoon morphology is supposed to be far from equilibrium as salt marshes have been reducing their extent during the last century (cf., Figure 7 later in the text).

[51] Region *c* covers the stable part of the theoretical curve. Points in this region are characterized by bottom elevation lower than the curve peak and bottom shear stress higher than the critical shear stress. The conceptual model predicts that points in this region belong to stable tidal flats.
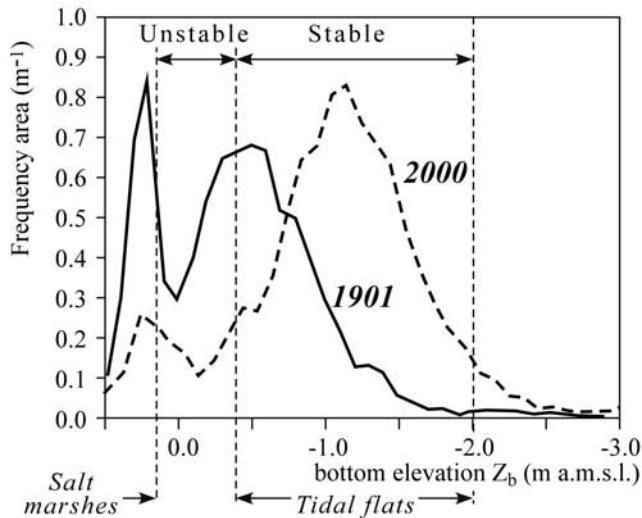
Figure 6. Frequency area distributions as a function of bottom elevation for the Southern Venice Lagoon (1901 and 2000 bathymetries).

Figure 5e shows the spatial distribution of these points inside the lagoon. They are uniformly distributed on tidal flats in the central part of the basin; only tidal channels, salt marshes, and sheltered regions are not covered by points, in agreement with the theoretical predictions. In addition, the morphological stability of region c can also be argued by the large amount of points falling in this region (79.5% of the total area covered by points in the strip falls into region c). Finally, region d comprises points with a bottom elevation deeper than $-2.00 \sim -2.5$ m a.m.s.l.. The conceptual model predicts no stable tidal flats in this region. Here the

bottom shear stress is lower than the critical shear stress (i.e., $E_S = 0$) and any deposition, however small, would rapidly infill areas deeper than $-2.00 \sim -2.5$ m a.m.s.l. Therefore points in region d can be either unstable or located in areas beyond the validity range of the model (for example, tidal channels). Figure 5f shows that the few points in region d (2.3% of total area covered by points in the strip) all belong to tidal channels and must be removed from the analysis.

[52] After removing all the points in regions 1 and 2, we evaluate the bottom-elevation probability-density-function (PDF) curve of the central-southern part of the Venice Lagoon. The curve, plotted in Figure 6, shows the minimum corresponding to elevations in the unstable range thus confirming that just a small fraction of the basin is characterized by these intermediate elevations, in agreement with the conceptual model.

3.2. 1901 Bathymetry

[53] A second simulation performed with the wind wave-tidal model uses the topography of the Venice Lagoon in 1901. A comparison between the 1901 and the 2000 bathymetries is shown in Figure 7. Contrary to the present lagoon morphology, in 1901 salt marshes covered most of the basin with a few areas occupied by tidal flats.

[54] The same wind and tidal conditions are applied to the 1901 bathymetry. After removing all points outside the strip enclosed between curves A and B of Figure 4, the frequency area distribution curve is obtained and plotted in Figure 6 where it is compared with the one obtained with the modern bathymetry. The minimum within the unstable range of elevations is even more evident in 1901 than in 2000. The peak of the distribution falls near the critical elevation, corresponding to the peak in the wave shear stress distri-
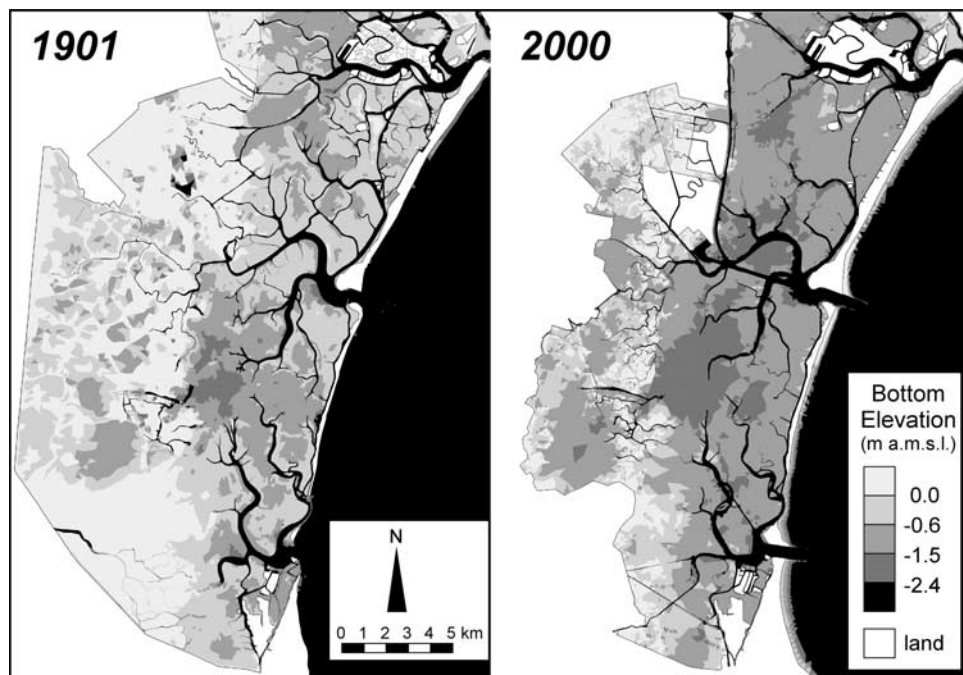
Figure 7. Bathymetry of the Venice Lagoon, Italy, in 1901 (left) and in 2000 (right). Elevation is in meters above the mean sea level (m a.m.s.l.) actually characterizing the North Adriatic Sea at the beginning and at the end of the last century, respectively.

bution. According to the conceptual model, this means that the average ratio of deposition rate to erosion rate was larger in 1901 than today. In fact, it is commonly stated that the construction, at the beginning of the 19th century, of the long jetties bounding the inlets is responsible for the considerable increase of the sediment volume that is exported to the ocean every year.

[55] Relative sea level rise (which includes subsidence), of about 23 cm for the Lagoon of Venice during the last century [Canestrelli and Battistin, 2006], had some influence on the deepening of tidal flats which according to Figure 6 is approximately 70 cm. However, in the context of the conceptual model, if the sediment supply does not vary, then an increase in water depth due to sea level rise is offset by a decrease in erosion that drives the tidal flat back to its equilibrium water depth.

[56] To study the impact of sea level rise on tidal flat equilibrium, we use the Exner equation that reads:

$$(1-n)\frac{\partial Z_{abs}}{\partial t} = D_S - E_S \quad (12)$$

where Z_{abs} denotes bottom elevation with respect to a fixed reference level and n denotes porosity. Noting that bottom elevation Z_b, with respect to mean sea level h_m, is given by $Z_b = Z_{abs} - h_m$, equation (12) can be rearranged to read

$$(1-n)\frac{\partial Z_b}{\partial t} = D_S - E_S - (1-n)R \quad (13)$$

where R is the rate of sea level rise, equal to $\partial h_m/\partial t$. Equilibrium condition, in the context of the conceptual model, is achieved when $\partial Z_b/\partial t = 0$ (that is, when bottom elevation does not change with respect to mean sea level), thus we have

$$D_S = E_S + (1-n)R \quad (14)$$

It is clear from equation (14) that sea level rise acts exactly as erosion does. A moderate sea level rise that does not overtake deposition will merely adjust the tidal flat-attracting point (S point in Figure 1) toward positions characterized by a smaller bed shear stress. The shift in equilibrium bed shear stress τ_{eq} can be easily estimated as follows.

[57] For the case of fine cohesive sediment, erosion rate is given by equation (11) with $\alpha = 1$, thus we write:

$$E_S + (1-n)R - D_S = E_{S0}(\tau_{eq}/\tau_{cr} - 1) + (1-n)R - D_S = 0 \quad (15)$$

In the absence of sea level rise (i.e., $R = 0$), equation (15) gives a different equilibrium bed shear stress, τ_{eq0}. Sea level rise acts to reduce equilibrium bed shear stress from τ_{eq0} to τ_{eq}

$$\Delta\tau_{eq} = \tau_{eq0} - \tau_{eq} = \frac{(1-n)\tau_{cr}}{E_{S0}}R \quad (16)$$

For the Venice Lagoon, $E_{S0} \approx 1-10 \times 10^{-8}$ m/s [Amos et al., 2004]. If we further assume that, since 1900 the sea level has risen at 2.3 mm/year ($R \approx 8 \times 10^{-11}$ m/s), equation (16) gives $\Delta\tau_{eq} \approx 0.0003-0.003$ Pa. According to data plotted in Figure 2, and considering the more severe estimate for $\Delta\tau_{eq}$ (i.e., $\Delta\tau_{eq} = 0.003$ Pa), the impact of sea level rise is to increase equilibrium water depth over tidal flats of less than 1 cm.

[58] Therefore the recorded tidal flats deepening (of approximately 70 cm) must be ascribed to a decrease in sediment supply rather than to a relative sea level rise, which only contributed to speed up this evolutionary trend.

4. Implications for the Long-Term Evolution of Shallow Tidal Basins

[59] The conceptual model proposed by Fagherazzi et al. [2006] and tested herein bears important consequences for the long term evolution of shallow tidal basins.

[60] Tidal basins are either river paleovalleys drowned after an increase in sea level or coastal areas sheltered by barrier islands and spits. In both cases, the tidal basin disconnects the flux of sediments from the incoming rivers to the ocean, by storing and releasing the alluvial and lagoonal sediments with its own specific dynamics. Tidal basins are seldom in equilibrium and are either in aggradation or in erosion depending on the balance between the sediment input from the rivers and the output to the ocean driven by tidal currents through the inlets. The alluvial and lagoonal sediments are continuously reworked in the basin by tidal currents and wind waves. Tidal currents are ultimately responsible for the formation of the channels through localized erosion [D'Alpaos et al., 2005] and control the overall sediment fluxes between the basin and the ocean, whereas the diffusive character of the sediment transport triggered by wind waves smoothes bottom topography and builds-up flat landforms that are typical of intertidal environments. In an aggradational setting, the initial topography of the basin, which can be relatively ragged in the case of a drowned fluvial valley, becomes more and more gentle in time because of the accumulation and redistribution of sediments at the bottom caused by wind waves. Sediment diffusion by wind waves increases as water depth decreases until, for elevations greater than Z_{c2}, we have the formation of extensive tidal flats. The tidal flat elevation is clustered in a narrow range that, as previously discussed, depends on the balance between erosion and sediment supply. If more sediment is accumulated in the basin, the peak of the frequency area distribution shifts toward higher elevations, (Figure 8a, Phase 1). We call this phase tidal flat accretion.

[61] Locally, that is, in areas far from the inlets and sheltered from wind waves, the maximum erosion rate E_{Smax} is small because of the reduced wave height (for example, points in region 1 of Figure 4). In these areas deposition rates may thus be larger than E_{Smax} and tidal flats shoal and form a salt marsh [Fagherazzi et al., 2006].

[62] With a larger sediment supply, the peak in area distribution reaches the critical elevation corresponding to the peak in the wave shear stress distribution. Any further net deposition of sediment cannot move the peak to the left, since lower elevations are unstable, and gives rise to new salt marshes in the basin and to an increase in salt marsh
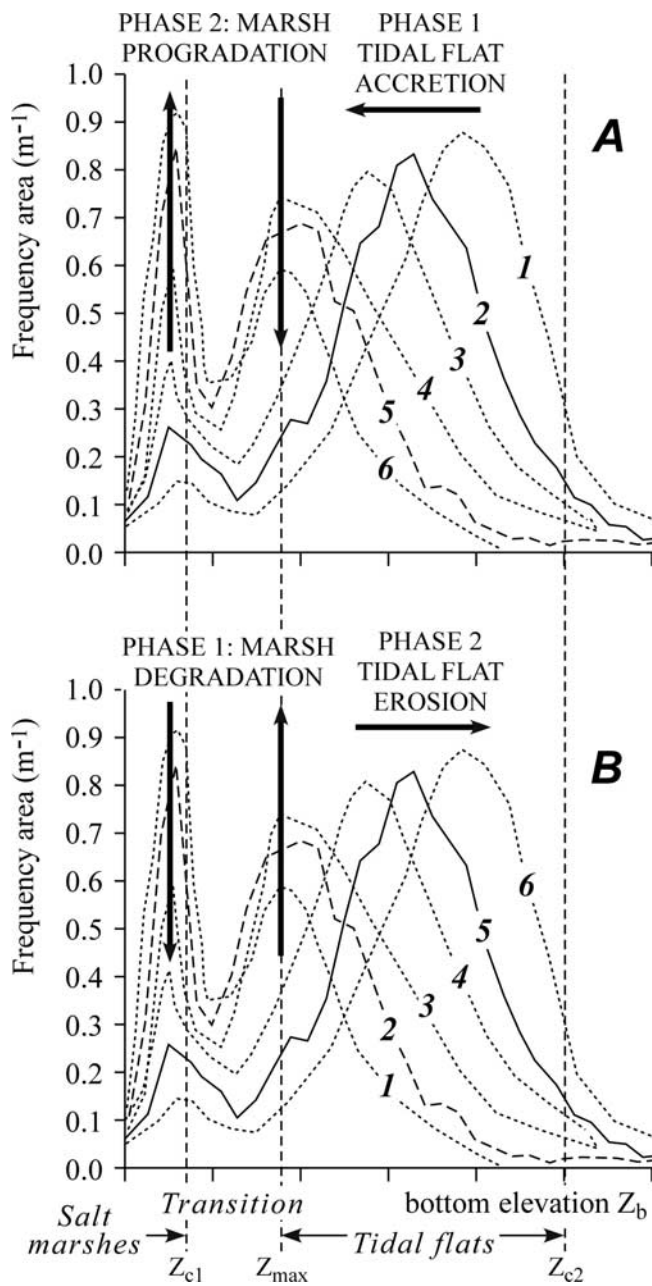
Figure 8. Long-term evolution of shallow tidal basins explained through the distribution of basin area as a function of elevation: (a) When there is a net accumulation of sediments in the basin a phase of tidal flat accretion (Phase 1) is followed by a phase of salt marsh progradation (Phase 2). (b) In a basin under erosion, a phase of marsh deterioration (Phase 1) is followed by a phase of tidal flat erosion (Phase 2). The solid line is the present area distribution in the southern Venice Lagoon; the dashed line is the area distribution in the southern Venice Lagoon in 1901 (see Figure 6); whereas the dotted lines represent hypothetical stages in time (from stage 1 to stage 6).

[63] In the same way, in a tidal basin under erosion, we can identify an initial phase in which salt marshes deteriorate and reduce their extension feeding with sediments the neighboring tidal flats which maintain an elevation near the critical one (Phase 1, Figure 8b, marsh deterioration). This stage is followed by a phase in which marshes have reduced their extension and the sediment supplied to tidal flats is not sufficient to balance tidal flat erosion. As a consequence, the average tidal flat elevation decreases (Phase 2 in Figure 8b, tidal flat erosion).
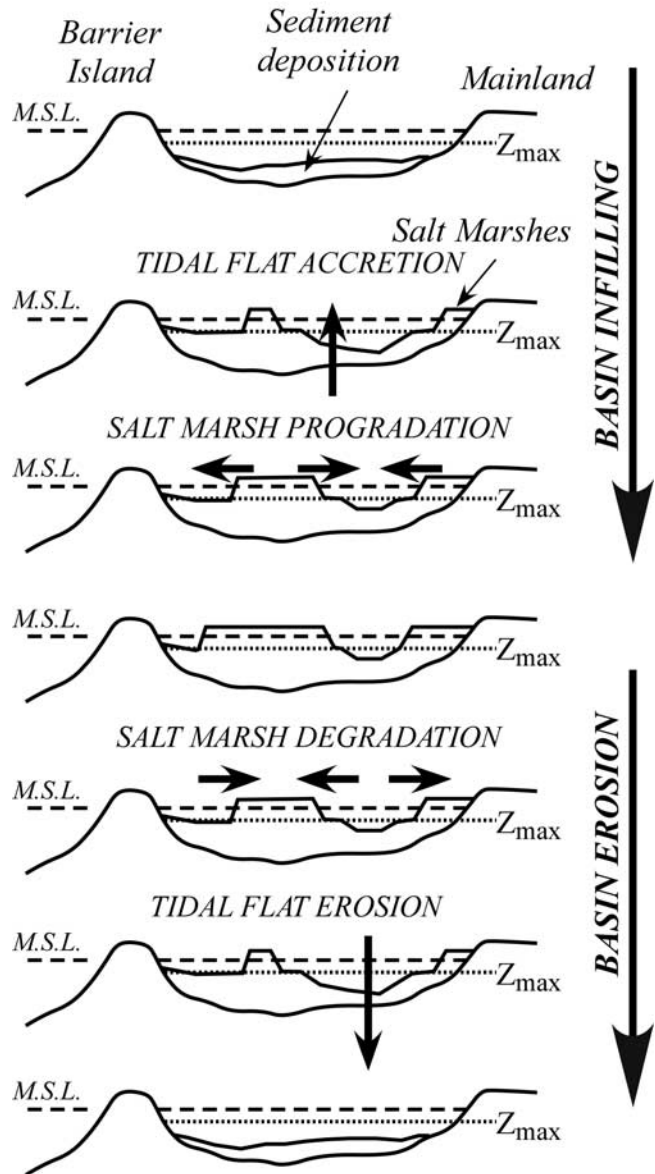
Figure 9. Conceptual model for the long-term evolution of shallow tidal basins. During basin infilling, a phase dominated by vertical tidal flat accretion is followed by a phase of horizontal salt marsh progradation. Similarly, during basin erosion, a phase of salt marsh degradation is followed by a phase of tidal flat erosion. The elevation of the tidal flats is always below or equal to the critical elevation Z_{max}.

area. The elevation of tidal flats remains locked around the critical elevation and the basin infilling only occurs by expansion of the salt marsh area. We call this phase salt marsh progradation (Figure 8a, Phase 2).

[64] The conceptual model of basin evolution is shown in Figure 9. When the overall deposition is larger than erosion, we have a vertical tidal flat accretion phase followed by an horizontal salt marsh progradation phase during which the tidal flats maintain an elevation equal or below the critical one ($Z_{\max}$). Conversely, when the overall erosion is larger than deposition, we have an initial salt marsh degradation phase followed by tidal flat erosion.

[65] In the light of the above discussion, we can interpret the morphological trends of the Venice Lagoon. The Southern lagoon in 1901 have a peak in the frequency of tidal flat elevation approximately at -0.5 m. Since in 1901 large areas of the Southern lagoon were encroached by salt marshes, we can deduce that $Z_{\max} = -0.5$ m is the critical tidal flat elevation and that at the beginning of the last century any loss (gain) in sediments was reflected in an increase (decrease) in marsh area.

[66] On the contrary, in 2000, the most frequent tidal flat elevation is approximately -1 m. This means that, at present, the basin is already in the phase of vertical tidal flat erosion and any further loss of sediments will further deepen the tidal flats and will ultimately lead to a smooth horizontal bottom with elevations around $-2 \sim -2.5$ m a.m.s.l.

[67] This trend correspond to the one shown in Figure 8b which includes the frequency area distributions of bottom elevations for the southern part of the Venice Lagoon in 1901 and 2000.

5. Conclusions

[68] In this work, the conceptual model explaining the mechanism leading to the appearance of tidal flats and salt marshes proposed by *Fagherazzi et al.* [2006] is validated through comparison with numerical results obtained with a two-dimensional wind wave-tidal model applied to the Lagoon of Venice. The model is forced with real tidal and meteorological conditions which are representative of typical, morphologically significant, stormy conditions for the Venice Lagoon.

[69] The computed bottom shear stresses plotted versus bottom elevation show a remarkable concentration of points around the theoretical curve predicted by the conceptual model. Moreover, an analysis of the spatial distribution of shear stresses demonstrates that points away from the theoretical curve (regions 1 and 2 in Figure 4) as well as points with a bottom elevation lower than the minimum bottom elevation predicted by the conceptual model for tidal flats (region *d* in Figure 4) do not meet model hypotheses as they are located in tidal channels or in fetch-limited areas. It is further shown that all points falling along the stable branch of the curve are indeed tidal flats, while the few points (less than 10% of total area) along the unstable branch are located on tidal flats close to salt marsh edges. Here the present lagoon morphology is presumably far from equilibrium because salt marshes are reducing their extension. The above result is also supported by the bottom-elevation PDF curve (Figure 6) which shows a minimum corresponding to elevations between tidal flats and salt marshes (i.e., in the unstable range of depths).

[70] The same conclusions are drawn from the analysis of the results of the second numerical simulation which uses the 1901 bathymetry of the Venice Lagoon characterized by a very different morphology with salt marsh area much larger than the present one.

[71] Based on the conceptual model and the computed frequency area curves, a framework that explains the long-term evolution of shallow tidal basins is finally proposed and discussed. In aggradational conditions, first tidal flats accrete until the critical elevation $Z_{\max}$ is reached, and then salt marshes expand. On the contrary, in an erosional condition, first salt marshes deteriorate and reduce their extension and then tidal flats deepen.

Notation

$\boldsymbol{c}_g = (c_{gx}, c_{gy})$ wave group celerity, m/s

D equivalent water depth, m

D_S sedimentation rate, m/s

D_{50} median grain diameter, m

E wave energy density, N/m

E_S rate of sediment erosion, m/s

$E_{S\max}$ maximum erosion rate, m/s

E_{S0} specific erosion rate, m/s

f_w wave friction factor

g gravitational acceleration, m/s^2

H wave height, m

h free surface elevation above mean sea level, m

h_m mean sea level, m

k wave number, m^{-1}

k_S Strickler bed roughness coefficient, m$^{1/3}$/s

n porosity

$\boldsymbol{q} = (q_x, q_y)$ flow rate per unit width, m^2/s

R sea level rise rate m/s

R_{ij} Horizontal Reynolds stresses (i, j = either x or y), m^3/s^2

S source term in the wave energy balance equation, N/ms

S_{bf} wave energy dissipated by bottom friction, N/ms

S_{brk} wave energy dissipated by breaking, N/ms

S_w wave energy generated by wind action, N/ms

S_{wc} wave energy dissipated by whitecapping, N/ms

t time, s

T wave period, s

u_m maximum horizontal orbital velocity at the bottom, m/s

Y effective water depth, m

Z_b bottom elevation above mean sea level, m

Z_{abs} bottom elevation with respect to a fixed reference level, m

Z_{c1} upper boundary depth of the unstable region, m

Z_{c2} lower boundary depth of the stable region, m

$Z_{\max}$ boundary depth between the stable and unstable regions, m

η wetted area per unit surface

ϕ angle between the current and the wave directions

ρ fluid density, kg/m^3

σ wave frequency, s^{-1}

τ_b maximum bed shear stress (waves and currents), N/m^2

τ_{bm} average bed shear stress (waves and currents), N/m^2

$\boldsymbol{\tau}_{b,curr} = (\tau_{bx}, \tau_{by})$ bed shear stress (tidal flow), N/m^2

$\boldsymbol{\tau}_{b,wave} = (\tau_{bx}, \tau_{by})$ bed shear stress (waves), N/m^2

τ_{cr} critical shear stress for sediment erosion, N/m^2

τ_{eq} equilibrium bed shear stress, N/m^2

τ_{max} bed shear stress corresponding to maximum erosion, N/m^2

$\boldsymbol{\tau}_w = (\tau_{wx}, \tau_{wy})$ wind shear stress, N/m^2

References

Allen, J. R. L. (2000), Morphodynamics of Holocene saltmarshes: A review sketch from the Atlantic and Southern North Sea coasts of Europe, *Quat. Sci. Rev.*, *19*, 1151–1231.

Allen, J. R. L., and M. J. Duffy (1998), Medium-term sedimentation on high intertidal mudflats and salt marshes in the Severn Estuary, SW Britain: The role of wind and tide, *Mar. Geol.*, *150*(1–4), 1–27.

Amos, C. L., A. Bergamasco, G. Umgiesser, S. Cappucci, D. Cloutier, L. DeNat, M. Flindt, M. Bonardi, and S. Cristante (2004), The stability of tidal flats in Venice Lagoon – The results of in-situ measurements using two benthic, annular flumes, *J. Mar. Syst.*, *51*(1–4), 211–241.

Beeftink, G. (1966), Vegetation and habitat of the salt marshes and beach plains in the south-western part of Netherlands, *Wentia*, *15*, 83–108.

Booij, N., R. C. Ris, and L. H. Holthuijsen (1999), A third-generation wave model for coastal regions: 1. Model description and validation, *J. Geophys. Res., [Oceans]*, *104*(C4), 7649–7666.

Canestrelli, P., and D. Battistin (2006), *1872–2004: La Serie Storica Delle Mare a Venezia*, edited by Canestrelli, and Battistin, I.C.P.S.M. Venice Italy, 208 pp.

Carniello, A., A. Defina, S. Fagherazzi, and L. D'Alpaos (2005), A combined wind wave-tidal model for the Venice Lagoon, Italy, *J. Geophys. Res.*, *110*, F04007, doi:10.1029/2004JF000232.

D'Alpaos, L., and A. Defina (1993), Venice Lagoon hydrodynamics simulation by coupling 2D and 1D finite element models, *Proceedings of the 8th Conference on Finite Elements in Fluids. New trends and Applications*, Barcelona (Spain), 20–24 September 1993, p. 917–926.

D'Alpaos, L., and A. Defina (1995), Modellazione matematica del comportamento idrodinamico di zone a barena solcate da una rete di canali minori, *Rapporti e Studi, Ist. Veneto di Scienze, Lettere ed Arti. XII*, p. 353–372.

D'Alpaos, A., S. Lanzoni, M. Marani, S. Fagherazzi, and A. Rinaldo (2005), Tidal network ontogeny: Channel initiation and early development, *J. Geophys. Res.*, *110*, F02001, doi:10.1029/2004JF000182.

D'Alpaos, A., S. Lanzoni, S. M. Mud, and S. Fagherazzi (2006), Modelling the influence of hydroperiod and vegetation on the cross-sectional formation of tidal channels, *Estuarine, Coastal Shelf Sci.*, *69*, 311–324, doi:10.1016/j.ecss.2006.05.002.

Defina, A. (2000), Two dimensional shallow flow equations for partially dry areas, *Water Resour. Res.*, *36*, 11, 3251–3264.

Defina, A. (2003), Numerical experiments on bar growth, *Water Resour. Res.*, *39*(4), 1092, doi:10.1029/2002WR001455.

Defina, A., L. D'Alpaos, and B. Matticchio (1994), A new set of equations for very shallow water and partially dry areas suitable to 2D numerical models, in *Proceedings of the Specialty Conference on "Modelling of Flood Propagation Over Initially Dry Areas"*, edited by P. Molinario and L. Natale, Milan (Italy), 29 June to 1 July 1994, American Society of Civil Engineers, New York, 72–81.

Dijkema, K. S. (1987), Geography of salt marshes in Europe, *Z. Geomorphol.*, *31*, 489–499.

Fagherazzi, S., and D. J. Furbish (2001), On the shape and widening of salt marsh creeks, *J. Geophys. Res., [Oceans]*, *106*(C1), 991–1003.

Fagherazzi, S., A. Bortoluzzi, W. E. Dietrich, A. Adami, S. Lanzoni, M. Marani, and A. Rinaldo (1999), Tidal networks: 1. Automatic network extraction and preliminary scaling features from digital elevation maps, *Water Resour. Res.*, *35*(12), 3891–3904.

Fagherazzi, S., L. Carniello, L. D'Alpaos, and A. Defina (2006), Critical bifurcation of shallow basin landforms in tidal flats and salt marshes, *Proc. Natl. Acad. Sci., U. S. A.*, *103*, 8337–8341, ISSN: 0027-8424, doi:10.1073/pnas.0508379103.

French, J. R., and D. R. Stoddart (1992), Hydrodynamics of salt-marsh creek systems – Implications for marsh morphological development and material exchange, *Earth Surf. Processes Landforms*, *17*(3), 235–252.

Hasselmann, K., et al. (1973), Measurements of wind-wave growth and swell decay during the Joint North Sea Wave Project (JONSWAP), *Dtsch. Hydrogr. Z.*, *12*(Suppl. A8), 1–95.

Marani, M., E. Belluco, A. D'Alpaos, A. Defina, S. Lanzoni, and A. Rinaldo (2003), On the drainage density of tidal networks, *Water Resour. Res.*, *39*(2), 1040, doi:10.1029/2001WR001051.

Mehta, A. J., E. J. Hayter, W. R. Parker, R. B. Krone, and A. M. Teeter (1989), Cohesive sediment transport, I: Process description, *Hydraul. Eng.*, *115*(8), 1076–1093.

Rinaldo, A., S. Fagherazzi, S. Lanzoni, M. Marani, and W. E. Dietrich (1999a), Tidal networks: 2. Watershed delineation and comparative network morphology, *Water Resour. Res.*, *35*(12), 3905–3917.

Rinaldo, A., S. Fagherazzi, S. Lanzoni, M. Marani, and W. E. Dietrich (1999b), Tidal networks: 3. Landscape-forming discharges and studies in empirical geomorphic relationships, *Water Resour. Res.*, *35*(12), 3919–3929.

Sanford, L. P., and J. P. Y. Maa (2001), A unified erosion formulation for fine sediments, *Mar. Geol.*, *1–2*, 9–23.

Silvestri, S., A. Defina, and M. Marani (2005), Tidal regime, salinity and salt marsh plant zonation, *Estuarine, Coastal Shelf Sci.*, *62*, 119–130, doi:10.1016/j.ecss.2004.08.010.

Soulsby, R. L. (1995), Bed shear-stresses due to combined waves and currents, in *Advances in Coastal Morphodynamics*, edited by M. J. F. Stive, J. Fredsoe, L. Hamm, R. L. Soulsby, C. Teisson, and J. C. Winterwerp, Delft Hydraulics, Delft, pp. 4-20–4-23.

Soulsby, R. L. (1997), *Dynamics of Marine Sands. A Manual for Practical Applications*, Thomas Telford, London, 248 pp.

Van Rijn, L. C. (1984), Sediment transport, Part II: Suspended load transport, *Hydraul. Eng.*, *110*(11), 1613–1641.

_____

L. Carniello, L. D'Alpaos, and A. Defina, Department IMAGE, University of Padova, Via Loredan 20, I-35131, Padova, Italy. (carniello@idra.unipd.it; dalpaos@idra.unipd.it; defina@idra.unipd.it)

S. Fagherazzi, Department of Geological Sciences and School of Computational Science, Florida State University, Tallahassee, FL 32301, USA. (sergio@csit.fsu.edu)